Switching of magnetic coupling by a structural symmetry change near the Mott transition in $Ca_{2-x}Sr_xRuO_4$

S. Nakatsuji
Department of Physics, Kyoto University, Kyoto 606-8502, Japan

Y. Maeno
Department of Physics, Kyoto University, Kyoto 606-8502, Japan
and CREST, Japan Science and Technology Corporation, Japan

(Received 24 February 2000)

We studied the structural, magnetic, and transport properties of the quasi-two-dimensional Mott transition system $Ca_{2-x}Sr_xRuO_4$. In the vicinity of the metal-nonmetal (M-NM) transition at $x \simeq 0.2$, we found a structural transition accompanied by a structural symmetry change with the instability point at $x_c \simeq 0.5$. The critical change across the structural transition in the temperature dependence of the susceptibility indicates a crossover of the metallic state, most likely from the nearly antiferromagnetic state next to the M-NM transition to the nearly ferromagnetic state around x_c. The latter evolves into the spin-triplet superconductor Sr_2RuO_4 ($x=2$) with enhanced paramagnetism. We argue that the competition between the structural instability and the ferromagnetism results in such a structural symmetry change with orbital degeneracy lifting, which induces the switching of magnetic coupling. In addition, a changeover from metallic to nonmetallic behavior was observed across the structural transition in the out-of-plane resistivity, which reveals highly anisotropic transport due to the quasi-two-dimensional electronic structure.

I. INTRODUCTION

The appearance of a wide range of ground states in the $4d$ transition metal oxides of ruthenates has recently attracted much research attention. By controlling both the bonding state in RuO_2 layers and the layer-stacking dimensionality, perovskite ruthenates exhibit various kinds of ground states such as spin-triplet superconductivity, itinerant ferromagnetism, antiferromagnetism, and the Mott insulating state.[1]

Among them, the quasi-two-dimensional $Ca_{2-x}Sr_xRuO_4$ provides a new type of Mott transition system that continuously connects the Mott insulator Ca_2RuO_4 with the spin-triplet superconductor Sr_2RuO_4.[2] The phase diagram has clarified the unusual variation of the ground state in the Mott transition route toward the spin-triplet superconductor, which consists of the following three regions as in Fig. 1.

First in region I ($0 \leqslant x < 0.2$), the metal-nonmetal (M-NM) transition occurs by varying either the Sr content or the temperature. In region II ($0.2 \leqslant x < 0.5$) near the M-NM transition, an antiferromagnetically (AF) correlated metallic state has been found at low temperatures, which we will refer to as the magnetic metallic (M-M) region. Moreover, the critical increase of low-temperature susceptibility observed near its region boundary at $x_c \simeq 0.5$ suggests a dramatic change of the ground state to a nearly ferromagnetic (FM) one, which evolves into the spin-triplet superconductor in region III ($0.5 \leqslant x \leqslant 2$).

In this paper, we report on the structural, magnetic, and transport studies of the metallic region in $Ca_{2-x}Sr_xRuO_4$. In the Ca-rich region near the M-NM transition, we found a structural transition possibly of second order with the zero-temperature instability point at x_c. A detailed analysis of the temperature dependence of the susceptibility has revealed that it is this transition that induces the magnetic crossover, most likely from the AF correlated state in the M-M region, to the nearly FM state around the instability point. The observed structural symmetry change may result in a variation in the shape and the effective filling of the triply degenerate bands through Jahn-Teller-type orbital rearrangement. We propose such a band splitting model to explain the magnetic crossover. The critical enhancement of the low-temperature susceptibility toward the structural instability point is ascribable to the result of the competition between the ferromagnetism and the Jahn-Teller instability. Finally, across the

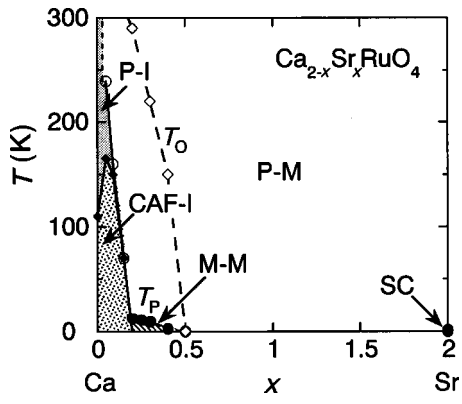

FIG. 1. Phase diagram of $Ca_{2-x}Sr_xRuO_4$ with abbreviations: P for paramagnetic, CAF for canted antiferromagnetic, M for magnetic, SC for superconducting phase, -M for metallic phase, and -I for insulating phase. The boundaries are characterized by the peak temperature T_P of susceptibility for the [001] component (solid circle), the metal-nonmetal transition temperature $T_{M\text{-}NM}$ (open circle) and the antiferromagnetic transition temperature T_N (solid diamond). T_O (open diamond) is the temperature below which the in-plane susceptibility starts to show twofold anisotropy.

structural transition, we observed a changeover from metallic to nonmetallic behavior in the out-of-plane resistivity, which reveals the highly anisotropic transport due to the quasi-two-dimensional electronic structure.

II. EXPERIMENT

We have succeeded in synthesizing polycrystalline samples and in growing single crystals of $Ca_{2-x}Sr_xRuO_4$ in the whole region of x. Details of the preparations will be described elsewhere.[3] The crystal structures were studied by powder x-ray diffraction analysis at room temperature. The results for the single crystals indicate no trace of any second phase. For polycrystalline samples, almost all the spectra were identified as single phase, except for minor peaks of CaO detected in several batches.

To determine the oxygen content, a thermogravimetric (TG) analysis was performed, in which powdered samples were heated up to 1200°C at a rate of 2°C/min in a 90% Ar+10% H_2 flow. All the results show one sharp decrease in the thermogravimetric weight around 440°C, corresponding to the decomposition reaction $Ca_{2-x}Sr_xRuO_{4+\delta} \rightarrow (2-x)CaO+xSrO+Ru+(1+\delta/2)O_2$. From these results, we determined δ values such as $-0.01(2)$ for the stoichiometric Ca_2RuO_4 (corresponding to S phase in Refs. 4–6) and 0.00(2) for $x=0.09$, 0.2, 1.0, and 2. As a result, all the members of $Ca_{2-x}Sr_xRuO_4$ essentially have 4.0 oxygen atoms per formula unit and the electronic configuration is $\{Kr\}4d^4$. Due to a large crystal field, Ru^{4+} ions should be in the low-spin configuration t_{2g}^4.

The electrical resistivity was measured by a standard four-probe dc method. Magnetization measurements from 330 K down to 1.8 K were made with a superconducting quantum interference device (SQUID) magnetometer equipped with a sample-stage rotator. For high-temperature measurements up to 700 K, we used a sample space oven inserted into the magnetometer.

III. RESULTS

A. Structural transition in region II

In Fig. 2, we display the results of x-ray diffraction measurements of powdered single crystals for $x=0.09$, 0.2, and 2. All diffraction spectra are similar to each other, reflecting the basic K_2NiF_4-type structure. Especially, the results of Sr_2RuO_4 ($x=2$) and $x=0.2$ agree with the same tetragonal symmetry. Meanwhile, the spectrum of $x=0.09$ shows weak but definite orthorhombicity with splitting between (hkl) and (khl) peaks. For example, the inset of Fig. 2 shows that the (110) peak of $x=0.2$ splits into (200) and (020) peaks of $x=0.09$. Accordingly, the result of $x=0.09$ is well indexed with an orthorhombic unit cell with a volume of $\sqrt{2}a_t \times \sqrt{2}a_t \times c_t$, where a_t and c_t are parameters for an $I4/mmm$ cell. This is a situation similar to the case of Ca_2RuO_4 ($x=0$) with an orthorhombic $Pbca$ symmetry.[4,5]

The cell parameters for all the regions are shown in Fig. 3. In order to obtain an overall view, we adopted the $I4/mmm$ cell for the tetragonal lattice, the same as that of Sr_2RuO_4, while for the orthorhombic one, $a/\sqrt{2}$ and $b/\sqrt{2}$ are given instead of a and b. At each composition, the parameters for single-crystalline samples agree well with those

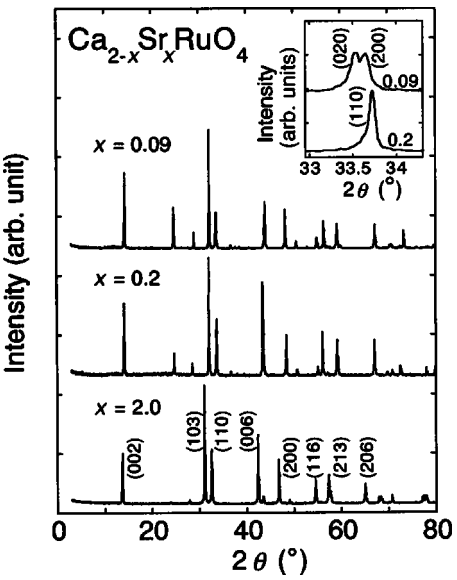

FIG. 2. X-ray (Cu $K\alpha$) diffraction spectra at room temperature for $Ca_{2-x}Sr_xRuO_4$ with $x=0.09$, 0.2, and 2. The inset shows that the (110) peak of $x=0.2$ splits into (020) and (200) peaks for $x=0.09$. For the inset, the $K\alpha 2$ component has been subtracted.

for polycrystalline ones. This indicates that the nominal composition x for each single crystal is essentially the same as the actual composition. Starting from Sr_2RuO_4, the volume decreases continuously with the Ca substitution owing to the smaller size of Ca^{2+} than that of Sr^{2+}. However, there are clear kinks without discontinuity in a, b, and c at $x=0.2$,

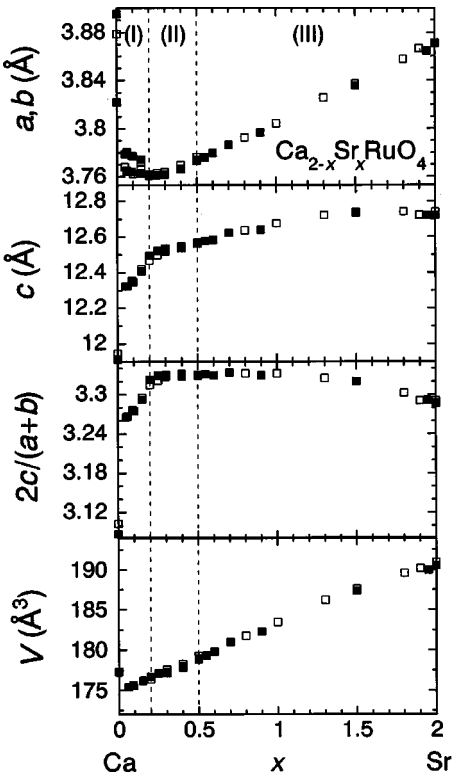

FIG. 3. Cell parameters a, b, c, $2c/(a+b)$, and unit cell volume V of $Ca_{2-x}Sr_xRuO_4$ at room temperature. The open and solid squares represent those parameters of polycrystalline and single-crystalline samples, respectively.

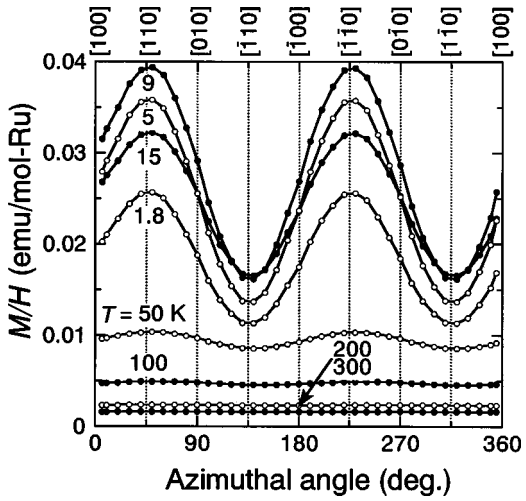

FIG. 4. In-plane anisotropy of the susceptibility under $\mu_0 H = 1$ T for $Ca_{1.8}Sr_{0.2}RuO_4$ at different temperatures.

where the splitting between a and b starts in region I. This clearly reveals a structural transition at room temperature from a tetragonal phase in regions II and III to an orthorhombic one in region I. Finally, near $x=0$, there is a large jump of the cell parameters probably due to a first-order structural transition, accompanied by the M-NM transition.[2] Therefore, the orthorhombic symmetry of the metallic phase in region I should be different from the orthorhombic $Pbca$ symmetry of the insulating phase.

In region II, the susceptibility $\chi(T)$ shows a broad peak at the temperature T_P, which characterizes the AF correlation in the M-M region.[2] At the same time, it exhibits another important aspect, namely, the in-plane anisotropy. The azimuthal angle dependence of the in-plane susceptibility at various temperatures is displayed in Fig. 4 for $x=0.2$. In comparison with the isotropic dependence at high temperatures, the anisotropy with twofold symmetry becomes evident as the temperature decreases. In order to quantify this temperature dependence, we define $R(T)$ as the susceptibility ratio of the easy axis [110] to the hard axis $[1\bar{1}0]$. Figure 5 shows that $R(T)$ for $x=0.2$ increases on cooling and reaches more than 200% below $T_P \simeq 12$ K. It is worth noting that, as in the inset of Fig. 5, $R(T)$ for $x=0.2$ starts to deviate from the isotropic value 100% at a characteristic temperature $T_O \simeq 290$ K.

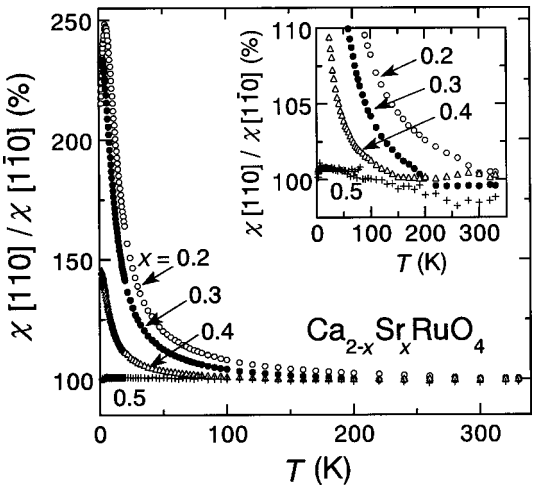

FIG. 5. Temperature dependence of the anisotropy ratio of the in-plane susceptibilities: $R(T)=\chi[110]/\chi[1\bar{1}0]$ for $Ca_{2-x}Sr_xRuO_4$ with $x=0.2$, 0.3, 0.4, and 0.5. The inset shows the appearance of the in-plane anisotropy at T_O.

Since the magnetic anisotropy reflects the structural symmetry,[7] the appearance of the twofold symmetry below T_O is ascribable to a structural transition from a high-temperature tetragonal to a low-temperature orthorhombic phase. We measured the in-plane azimuthal dependence of the susceptibility at various temperatures also for $x=0.3$, 0.4, 0.5, and 0.7. The twofold symmetry was found only in region II. From the $R(T)$ plots shown in Fig. 5, we determined T_O as 220 K for $x=0.3$, 150 K for 0.4, and below 1.8 K for 0.5 and 0.7. Plotting the variation of T_O in the phase diagram of Fig. 1, we notice that the T_O line crosses room temperature around $x=0.2$. Quite consistently, it is at this point where the structural transition was detected by the x-ray diffraction measurement. In addition to the strong shrinkage of the c axis in Fig. 3, the a and b axes start to elongate and split in region I. Therefore, we conclude that across the T_O line, a structural transition occurs from a tetragonal phase in the Sr-rich and high-temperature region to an orthorhombic phase in the Ca-rich and low-temperature region, involving the lattice flattening.

This transition is also detected as kinks in the resistivity data $\rho_{ab}(T)$ and $\rho_c(T)$ [see Fig. 8 for $\rho_{ab}(T)$ of $x=0.2$ and the inset of Fig. 9(a) for $\rho_c(T)$ of $x=0.2$ and 0.4]. The absence of the thermal hysteresis at these kinks suggests that this transition should be of the second order. The decrease of $\rho_c(T)$ and increase of $\rho_{ab}(T)$ below T_O are consistent with the lattice flattening. This will weaken the hybridization between the in-plane Ru $4d$ orbitals, while supporting coherent hopping between layers.

Neutron powder diffraction measurements have recently been performed for samples with $x=0.1$, 0.2, 0.5, and 1.0.[8] The results confirm that the second-order structural transition from a high-temperature tetragonal to a low-temperature orthorhombic phase occurs at T_O, inducing the lattice flattening owing to orthorhombic deformation of RuO_6 octahedra as well as their tilting. Details of the results will be described elsewhere.[8]

Another important point is that T_O decreases with x and finally goes down to zero at $x=0.5$ as in Fig. 1. This suggests that $x_c \simeq 0.5$ should be the instability point at absolute zero, in other words, the quantum critical point of the second-order structural transition.

B. Evolution of the temperature dependence of the susceptibility

In the entire metallic region, the $\chi(T)$ curve shows a systematic variation with x. We define the susceptibility $\chi \equiv M/H$ at low enough fields (up to 1 T) where the magnetization M shows linear dependence on the field H. In Figs. 6(a) and 6(b), we display the in-plane $\chi_{ab}(T)$ curves for single-crystalline samples in regions II and III, respectively. The inverse susceptibilities measured up to 700 K for polycrystalline samples in regions II and III are also given in the insets of Fig. 6(a) and Fig. 6(b), respectively.

In order to clarify the evolution of the temperature dependence, we performed a Curie-Weiss (CW) analysis on both

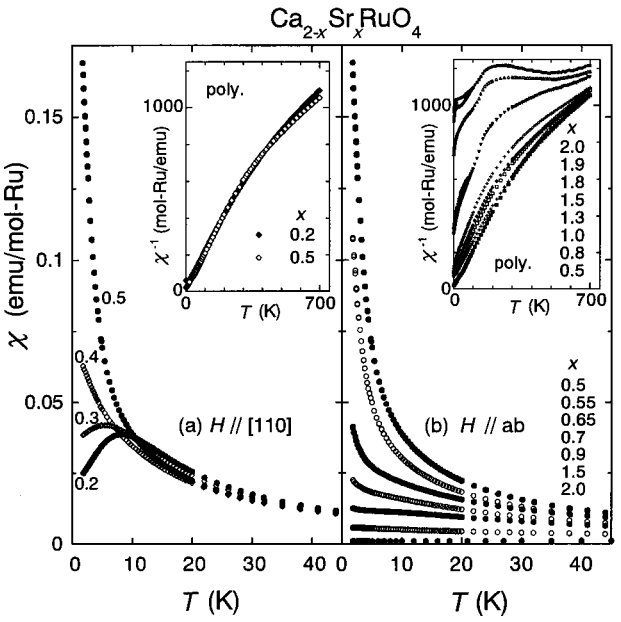

FIG. 6. Temperature dependence of the in-plane susceptibility for $Ca_{2-x}Sr_xRuO_4$ with different values of x (a) in region II for the [110] component and (b) in region III. For both regions, the zero-field-cooled (ZFC) and field-cooled (FC) curves agree very well. The insets for (a) and (b) display the inverse susceptibility of polycrystalline samples in regions II and III, respectively. For polycrystalline samples only around $x=2$, the difference between the ZFC and FC curves can be seen at low temperatures. This is probably due to a small inclusion ($<0.04\%$) of ferromagnetic impurity $Ca_{1-x}Sr_xRuO_3$.

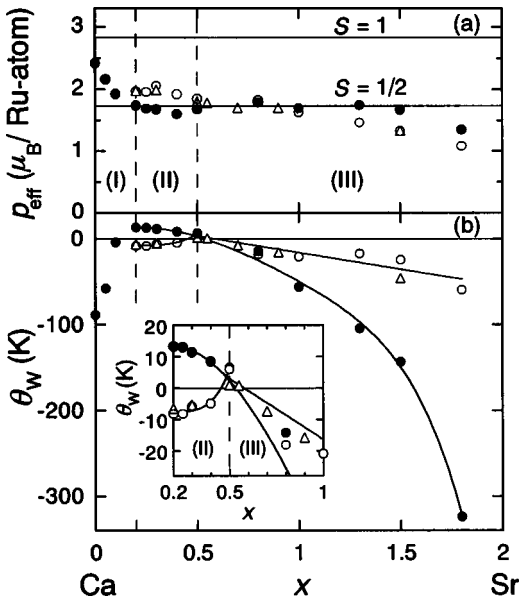

FIG. 7. Curie-Weiss parameters against the Sr content x in $Ca_{2-x}Sr_xRuO_4$. The solid and open circles correspond to the results of polycrystalline samples for the high-temperature and the low-temperature fitting regions, respectively. The open triangles represent the low-temperature fitting results of single crystals for the ab-plane component in region III and $[1\bar{1}0]$ component in region II. In the panel (a), the solid horizontal lines correspond to the effective Bohr magnetons with $S=1/2$ and 1. The inset in the panel (b) is an enlarged figure for region II. The solid curves are guides to the eye.

polycrystalline and single-crystalline samples. The analyses were made in a high-temperature (HT) fitting region, 300–700 K for polycrystalline samples, and in a low-temperature (LT) fitting region, 50–330 K for both polycrystalline and single-crystalline samples. For the samples in region II, we restricted the LT region from 50 K up to (T_O-20) K below the structural transition. Since Ca_2RuO_4 exhibits a first-order transition around 350 K,[8,9] we performed the fitting for the HT region between 380 and 700 K. We adopted the fitting formula as

$$\chi=\chi_0+\frac{C}{T-\Theta_W}. \tag{3.1}$$

Here, χ_0 is a temperature-independent term, C is the Curie constant, and Θ_W is the Weiss temperature. The effective Bohr magneton $p_{\rm eff}$ was derived from the formula

$$C=\frac{N_A p_{\rm eff}^2 \mu_B^2}{3k_B}, \tag{3.2}$$

where N_A, μ_B, and k_B are Avogadro's number, the Bohr magneton, and Boltzmann's constant. For $x=1.9$ and 2, the fitting was not successful because χ is almost constant up to 700 K.

Except for near $x=2$, χ_0 has values only of the order of 10^{-4} emu/mol Ru, and is negligible in comparison with the low-temperature susceptibility $\chi(0)$ at 1.8 K.[2] Hence, we will focus on the fitting results of $p_{\rm eff}$ and Θ_W, which are summarized in Figs. 7(a) and 7(b), respectively. As shown by band calculations,[10] the states at the Fermi level (E_F) in Sr_2RuO_4 are mainly composed of $4d$ t_{2g} bands. Basically, this configuration should not change throughout the system, and thus the itinerant t_{2g} spins are responsible for the dominating CW term in Eq. (3.1).

Figure 7(a) shows a systematic x dependence of $p_{\rm eff}$. First, Ca_2RuO_4 $(x=0)$ has the largest $p_{\rm eff}$ with almost 80% of the expected value for the $S=1$ configuration. As the system goes away from the insulating phase, $p_{\rm eff}$ decreases rapidly in region I and finally becomes almost constant in the region $0.2\leqslant x\leqslant 1.5$. Quite interestingly, the results in this region, especially the HT results for polycrystalline samples (solid circles), are close to the value corresponding to $S=1/2$ spin. Given Hund's coupling in the t_{2g} band, the $S=1$ configuration is naturally expected. In addition to being a metal, the enhanced spin fluctuations due to the structural two dimensionality and the orbital degree of freedom are probably responsible for the reduced $p_{\rm eff}$. However, this mechanism alone does not explain why the effective S remains close to 1/2.

According to the conventional analysis, positive and negative values of Θ_W indicate the strength of ferromagnetic and antiferromagnetic interactions, respectively. While for Ca_2RuO_4 this rule works well and $\Theta_W\simeq 90$ K has the same order of magnitude as its Néel point $T_N=110$ K, a slight Ca substitution reduces the absolute value of Θ_W much faster than that of T_N. However, the increase of negative Θ_W is still qualitatively consistent with the decrease of AF coupling of the order of T_N in region I.

In region III, Θ_W for both HT and LT regions also has

negative values, but increases with decreasing x. LT results for single crystals (open triangles) are consistent with those for polycrystalline samples (open circles). In general, a fairly large value of Θ_W is necessary to reproduce the almost temperature-independent behavior of Eq. (3.1). Accordingly, near the Pauli paramagnetic Sr_2RuO_4, Θ_W has a large negative value, and owing to the evolution of Curie-Weiss behavior the magnitude decreases rapidly with the Ca substitution. Thus, the negative value of Θ_W in this region does not indicate the strength of the AF coupling. Alternatively, according to the self-consistent renormalization (SCR) theory,[11] this increase in negative Θ_W to zero can be well understood as the result of the evolution of FM spin fluctuations. The band narrowing due to the Ca substitution must be the main cause of this FM coupling, as we will discuss in Sec. IV B 2.

Here, it is also important to stress that both HT and LT results show qualitatively the same feature that Θ_W with negative values increases with the Ca substitution. Furthermore, they finally coincide around $x=0.8$ and approach zero together near $x=0.5$.

Once the system enters region II, however, Θ_W for each fitting region starts to show definitely a different x dependence, as shown in the inset of Fig. 7(b). While the result for $T>T_O$ (solid circles) increases continuously on the extended track from region III, Θ_W for $T<T_O$ of both polycrystalline samples (open circles) and the $[1\bar{1}0]$ component of single-crystalline samples (open triangles) stops increasing at $x=0.5$ but starts to decrease in region II. Notably, Θ_W for $T<T_O$ has a negative value with the same order of magnitude as T_P. This sign reversal of Θ_W across T_O indicates that *the structural transition induces a change of magnetic coupling*.

In the ground state, this change becomes evident; it is at $x_c \simeq 0.5$ that both Θ_W in region III and T_P in region II vanish so that $\chi(0)$ critically enhances as shown in Fig. 6. This criticality indicates that the ground-state magnetism drastically changes at the structural instability. The continuous increase of the HT result of Θ_W across $x=0.5$ suggests that without the structural transition, $\chi(0)$ would keep diverging with decreasing x. Therefore, the critical point at $x_c \simeq 0.5$ should be very close to a FM instability. In reality, however, the AF correlation takes over toward the Mott transition in the M-M region. Here, the negative Θ_W as well as T_P must be the indicator of the strength of the AF coupling. Thus, it is natural to consider that the structural transition halts the growth of the FM instability and switches on the AF coupling.

C. Anisotropic transport properties

Reflecting the quasi-two-dimensional structure, the temperature dependence of the resistivity $\rho(T)$ is quite anisotropic. Figure 8 presents the temperature-dependent part of the in-plane resistivity: $\rho_{ab}(T)-\rho_{ab}(0)$ measured down to 0.3 K for various values of x. All curves show metallic behavior (i.e., $d\rho/dT>0$). In fact, at low temperatures, $\rho_{ab}(T)$ are less than the Mott-Ioffe-Regel (MIR) limit of metallic conduction of about 200 $\mu\Omega$ cm for Sr_2RuO_4,[12] which suggests coherent metallic transport within the plane. As can be seen in Fig. 8, $\rho_{ab}(T)-\rho_{ab}(0)$ increases quite systematically with the Ca substitution. Because the temperature-dependent term is basically determined by inelastic scattering, which becomes severe for a narrow band metal with high $N(E_F)$, this increase is consistent with the band narrowing with the Ca substitution. In addition, $\rho_{ab}(T)-\rho_{ab}(0)$ for $x=0.2$ shows a steep decrease below $T_P \simeq 12$ K. This should come from a reduction of the spin scattering by the formation of AF short-range order in the M-M region.[2]

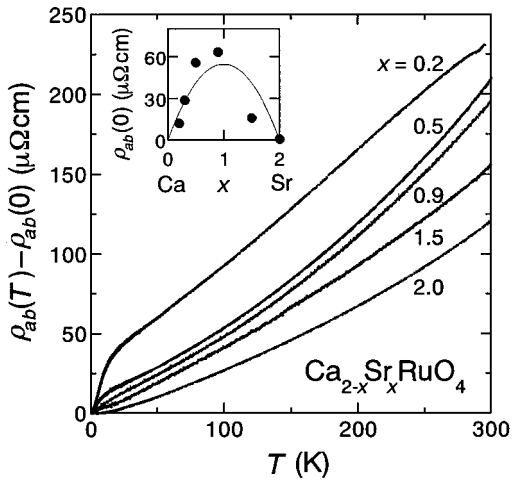

FIG. 8. Temperature dependence of the in-plane resistivity $\rho_{ab}(T)$ for $Ca_{2-x}Sr_xRuO_4$ with different values of x. The inset shows the x dependence of the in-plane residual resistivity $\rho_{ab}(0)$. The solid curve represents a fit to the Nordheim law.

The x dependence of the residual resistivity $\rho_{ab}(0)$ is presented in the inset of Fig. 8. In contrast with the continuous increase of $\rho_{ab}(T)-\rho_{ab}(0)$, $\rho_{ab}(0)$ has a peak around $x=1.0$, which is qualitatively consistent with the Nordheim law. The Nordheim formula $Ax(x-2)$ roughly fits the x dependence of $\rho_{ab}(0)$, as indicated by the solid curve with $A=54$ $\mu\Omega$ cm. This result strongly implies that the randomness intrinsic to the Ca substitution is responsible for the residual resistivity in this system.

In comparison with the metallic behavior of the in-plane component, the out-of-plane resistivity $\rho_c(T)$ is less temperature dependent and in some cases even nonmetallic (i.e., $d\rho/dT<0$). In order to show the temperature dependence clearly, we display $\rho_c(T)$ normalized by the values at 300 K: $\rho_c(T)/\rho_c(300\ \mathrm{K})$ in Fig. 9(a). All of them were measured down to 0.3 K. Here $\rho_c(300\ \mathrm{K})$ hardly depends on x and remains within 28 ± 3 mΩ cm for all x.

The MIR limit for the metallic c-axis conduction of Sr_2RuO_4 is estimated to be about 4 mΩ cm.[13] While the order of the limit should not be changed in this isostructural system, all the results of $\rho_c(T)$ are one order of magnitude higher than the limit except for Sr_2RuO_4. Therefore, the metallic behavior observed in the region $0.15 \leqslant x < 0.5$ is not attributable to the coherent conduction in the band picture. Instead, we consider here the diffusion and thermally assisted hopping processes for the transport mechanism. In both processes, quasiparticles hop between layers with a jumping frequency τ_c^{-1}, and the out-of-plane resistivity reads

$$\rho_c = [N(E_F)e^2 l^2 \tau_c^{-1}]^{-1}, \tag{3.3}$$

where $N(E_F)$ is the density of states at E_F, e is the elementary charge, and $D=l^2\tau_c^{-1}$ is the diffusion coefficient with a jumping (interlayer) distance l.

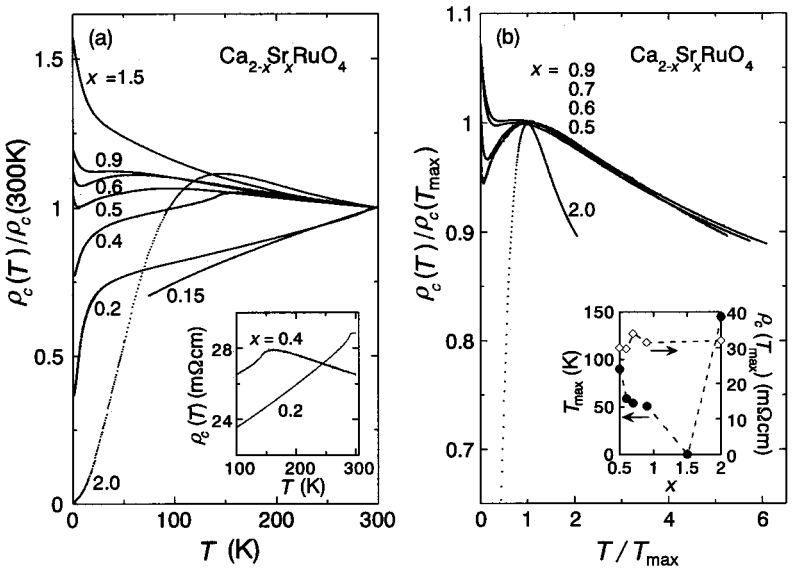

FIG. 9. (a) Temperature dependence of the out-of-plane resistivity $\rho_c(T)$ normalized by the values at 300 K for $Ca_{2-x}Sr_xRuO_4$ with different values of x. For $x=0.15$, the data are shown only above the M-NM transition point ~ 70 K. The inset illustrates the crossover at T_O for $x=0.2$ and 0.4. (b) The variation of $\rho_c(T)/\rho_c(T_{max})$ against T/T_{max} for several values of x in region III. The inset displays the x dependence of T_{max} (solid circle) and $\rho_c(T_{max})$ (open diamond).

$\rho_c(T)/\rho_{ab}(T)$ shows large anisotropy throughout the system. For example, the values for $x=0.2$, 0.9, 1.5, and 2 are 120, 130, 160, and 230 at 300 K and 780, 600, 2300, and 930 at 2 K, respectively. Therefore, the Fermi surface in this system must be remaining in almost cylindrical topology as that of Sr_2RuO_4. Consequently, the interlayer transfer integral t_c should be so small that the in-plane scattering becomes a dominant process for the c-axis transport. In this case, one can write the jumping rate as[13–16]

$$\tau_c^{-1}=t_c^2\tau_{ab}/\hbar^2, \tag{3.4}$$

where τ_{ab}^{-1} is the in-plane scattering rate and $h=2\pi\hbar$ is the Plank constant. From this equation, one can easily understand that even with this incoherent mechanism, ρ_c shows metallic behavior when ρ_{ab} is coherent so that τ_{ab}^{-1} becomes smaller on cooling. Hence, the metallic behavior in $0.15\leqslant x<0.5$ should arise from this mechanism.

The thermally assisted hopping process takes place when the thermal energy k_BT is much larger than the effective bandwidth W_c for the c-axis transport. In this case, the jumping rate can be expressed as[13]

$$\tau_c^{-1}=\tau_{c0}^{-1}\exp[-(\alpha W_c/k_BT)^n], \tag{3.5}$$

where α is a numerical factor and n depends on the dimensionality of the hopping. This process explains the nonmetallic behavior at high temperatures.

First in region I, $\rho_c(T)$ for $x=0.15$ is metallic at all the temperatures measured down to the M-NM transition temperature of about 70 K. However in region II, a clear changeover from nonmetallic to metallic behavior has been observed across T_O on cooling. [See the inset of Fig. 9(a) for $x=0.2$ and 0.4.] As we discussed in Sec. III A, the structural transition at T_O involves the lattice flattening, which should enhance the interlayer coherence by enlarging t_c. In contrast with the nonmetallic behavior due to the thermally assisted hopping at high temperatures, this increase in t_c by the transition must stabilize the diffusive hopping process below T_O, and thus more strongly metallic behavior appears with the Ca substitution.

In region III, however, the crossover in the temperature dependence occurs even without a structural transition, forming a maximum at T_{max}. Figure 9(b) demonstrates a scaling with the normalized axes $\rho_c(T)/\rho_c(T_{max})$ and T/T_{max} in $0.5\leqslant x\leqslant 0.9$. The inset of Fig. 9(b) illustrates the x dependence of T_{max} and $\rho_c(T_{max})$. Here $\rho_c(T_{max})$ stays almost constant at around 32 $m\Omega$ cm, consistent with the result of the pressure dependence for Sr_2RuO_4.[13]

In this case, since the thermally assisted hopping becomes effective when k_BT is larger than $W_c=4t_c$, the crossover temperature T_{max} should be roughly proportional to t_c. In fact, this expectation is consistent with several observations. First, given this assumption, Eq. (3.5) qualitatively explains the nearly universal temperature dependence above T_{max} as in Fig. 9(b).[17] Second, on this assumption, T_{max} shown in the inset of Fig. 9(b) indicates that W_c increases with decreasing x from 0.9 to 0.5. This is quite consistent with the expected enhancement in t_c due to the shrinkage of the interlayer distance $l=c/2$ as shown in Fig. 3. Moreover, the extension of the metallic region below T_{max} toward $x=0.5$ is also understandable by Eq. (3.4) with this increase in t_c. Finally, Eq. (3.5) may reproduce the nearly constant $\rho_c(T_{max})$ in this region, as discussed in Ref. 13.

Although the metallic region becomes wider with higher T_{max} as x changes from 1.5 to 0.5, the incoherent conduction at low temperatures still remains even at $x=0.5$. This may be due to an anisotropic weak localization effect by disorders in (Ca/Sr)O layers, which basically retains the coherent conduction in RuO_2 layers. Once the structural transition occurs in region II, however, $\rho_c(T)$ finally becomes metallic with a strong decrease at low temperatures.

On the other hand, in this region III, T_{max} decreases rapidly from $x=2$ to 1.5. The Ca substitution for Sr_2RuO_4 introduces not only randomness in SrO layers, but also distortion in RuO_2 layers. Actually, a recent powder neutron diffraction study confirms that the Ca substitution drives the rotation of RuO_6 octahedra along the c axis, which is absent in Sr_2RuO_4.[8] Hence, this rotational distortion as well as the

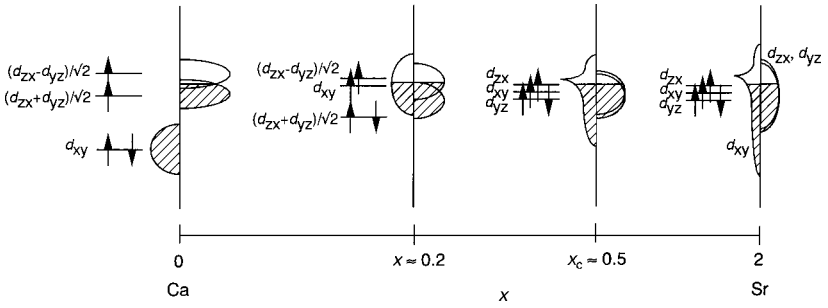

FIG. 10. Schematic variation of the electronic configuration in $Ca_{2-x}Sr_xRuO_4$ according to the band splitting model.

localization effect due to the randomness may be correlated with the incoherent $\rho_c(T)$ at $x=1.5$.

To summarize this section, we confirmed by the above analyses that the *c*-axis transport in this system is dominated by the hopping process, which systematically changes from the diffusive metallic hopping to the thermally assisted one with the Sr content x and the temperature, characterized by the small t_c ($\sim$ several 10 K) due to the quasi-two-dimensional electronic structure.

IV. DISCUSSION

A. Origin of the magnetoelastic coupling in Ca_2RuO_4

To understand those rich and unusual phenomena in $Ca_{2-x}Sr_xRuO_4$, we will discuss the variation of the ground-state magnetism and electronic structure. First, let us look into the Mott insulator Ca_2RuO_4. The neutron diffraction measurement by Braden *et al.*[5] has revealed strong magnetoelastic coupling in Ca_2RuO_4. They reported severe flattening as well as tilting of RuO_6 octahedra on cooling toward its Néel temperature. The in-plane oxygen O(1) distance elongates along the *b* axis of the *Pbca* unit cell, while the Ru–apical-oxygen O(2) bond shortens. However, once the staggered moment starts to align along the *b* axis, both flattening and tilting of RuO_6 octahedra saturate at lower temperatures.

Although the flattening of octahedra may be understood simply by the Jahn-Teller effect,[18] in order to explain the strong magnetoelastic coupling, we have to take account of spin-orbit coupling. Since the flattening induces a distinct orthorhombic crystal field, the t_{2g} orbitals split into three nondegenerate ones such as $d_{x_o^2-y_o^2}$ with the lowest energy, $d_{z_o x_o}$ in the middle, and $d_{y_o z_o}$ with the highest energy. Here, the x_o, y_o, and z_o axes correspond to the *a*, *b*, and *c* axes of the orthorhombic *Pbca* unit cell, respectively. [If we take the x and y axes along the in-plane Ru-O bonds as in the *I*4/*mmm* cell, $d_{x_o^2-y_o^2}$, $d_{y_o z_o}$, and $d_{z_o x_o}$ are transformed into d_{xy}, $(d_{zx}-d_{yz})/\sqrt{2}$, and $(d_{zx}+d_{yz})/\sqrt{2}$, respectively.] Basically, the tilting of RuO_6 octahedra along the *b* axis also stabilizes the above configuration, generating the orthorhombic crystal field by the second-nearest oxygens from a Ru ion. In this situation, the second-order perturbation theory for the spin-orbit coupling allows us to deduce that the b_o axis should become the easy axis of the spin alignment, which agrees with the observation of Braden *et al.*[5]

At the same time, since the shortening of the out-of-plane Ru-O bond is nearly twice as much as the elongation of the in-plane one, the $d_{x_o^2-y_o^2}$ or d_{xy} orbital should have much lower energy than the other two orbitals. Given the four electrons in the t_{2g} orbitals, such electronic structure may well realize a half-filled configuration at E_F [with two electrons in $(d_{zx}-d_{yz})/\sqrt{2}$ and $(d_{zx}+d_{yz})/\sqrt{2}$ orbitals as shown in Fig. 10], which favors AF superexchange coupling between neighboring spins. As a result, the orthorhombic distortion enhanced toward T_N stabilizes both the superexchange interaction and spin-orbit coupling in the Néel state. In this sense, the observed strong magnetoelastic coupling should be a cooperative phenomenon involving Jahn-Teller effect, superexchange, and spin-orbit coupling.

B. Ground-state crossover in the metallic region

1. Electronic configuration of Sr_2RuO_4

NMR studies have revealed that Sr_2RuO_4 exhibits exchange-enhanced paramagnetism with a local ferromagnetic coupling between in-plane spins at neighboring sites.[19,20] The origin of this coupling should consist in the electronic configuration. Because the out-of-plane Ru-O bond is longer than the in-plane ones, d_{xy} should have slightly different energy among the t_{2g} orbitals. However, the two-dimensional spreading d_{xy} forms a γ band wide enough to degenerate with the $d_{yz,zx}$ orbitals that produce rather narrow α and β bands, reflecting their one-dimensional networks.[10] Consequently, the Ru^{4+} t_{2g} band provides the electronic configuration of *four electrons in the triply degenerate band*. In addition, according to the band structure calculation,[10] the γ band has a large peak in the density of states (DOS) near E_F due to van Hove singularity (vHS), and results in a strongly asymmetric DOS of the overall t_{2g} band.

According to the theories on ferromagnetism in strongly correlated systems,[21] such an asymmetric DOS with a strong peak near E_F favors ferromagnetism for its ground state, while a symmetric, half-filled band stabilizes antiferromagnetism. Although the electronic configuration of Sr_2RuO_4 nearly satisfies the former condition, no substantial FM fluctuation has been detected so far. It is probably because of the rather low $N(E_F)$ that the FM fluctuations are not well developed to a wide range but remain local so as to realize the exchange-enhanced paramagnetism.[22]

We note that a recent inelastic neutron scattering measurement has revealed the existence of incommensurate spin fluctuations located at $(\pm 0.6\pi/a, \pm 0.6\pi/a, 0)$.[23] This is consistent with the prediction of nesting instability between α and β bands by a band structure calculation.[24] One dimensionality of the $d_{yz,zx}$ orbital network results in this nesting

effect. For the superconductivity, however, we speculate that the local ferromagnetic coupling mentioned above possibly stabilizes the spin-triplet pairing of Sr_2RuO_4, while the incommensurate spin fluctuations may have a minor or even an adverse effect. Mazin and Singh examined competition between *p*- and *d*-wave superconductivity by a calculation including both incommensurate and FM spin fluctuations, and drew a similar conclusion.[24,25]

2. Band splitting model

The Ca substitution in Sr_2RuO_4 brings about the critical enhancement of the low-temperature susceptibility toward $x=0.5$, which suggests that the structural instability point at $x_c \simeq 0.5$ should be close to a FM instability. In contrast, it is the AF correlation that becomes substantial in the M-M region at $x<0.5$. For the simplified picture of this switching of magnetic coupling, we propose the *band splitting model*, which is schematically illustrated in Fig. 10. In this model, the changes in the shape and filling of the band are vital to control the magnetism.

First, let us discuss the origin of the evolution of the FM correlation toward x_c in region III. While Sr_2RuO_4 has no structural distortion, the Ca substitution stabilizes and enhances the rotational distortion of RuO_6 octahedra along the *c* axis, as we mentioned in Sec. III C. As a consequence, the rotational distortion causes the following two main effects to enhance the FM coupling.

One is the band narrowing which enlarges $N(E_F)$. The distortion weakens the orbital hybridization and reduces the bandwidth. At the same time, since the structural symmetry remains tetragonal in region III, the crystal field symmetry around a Ru ion should be basically the same. Thus, the Ca substitution will neither lift the triple degeneracy of the bands nor blunt the vHS. Therefore, the system should keep basically the same asymmetric DOS which favors ferromagnetism. Additionally, the band narrowing will enhance the vHS, thereby $N(E_F)$ as well, so that the FM coupling gets stronger by the Stoner mechanism. This tendency is consistent with results by a recent mean-field theory based on the band structure of Sr_2RuO_4.[26]

Second, the rotation of octahedra will produce a stronger hybridization between d_{yz} and d_{zx}, which weakens the one-dimensional nature of α and β bands. Thus the nesting of these bands, the origin of the incommensurate spin correlation in Sr_2RuO_4, may become weaker with decreasing *x*. As a result, rotational distortion should develop the FM coupling from the enhanced paramagnetism of Sr_2RuO_4.

In the M-M region, however, the triple degeneracy must be lifted by the structural transition. The twofold anisotropy of the in-plane susceptibility below T_O indicates the broken tetragonal symmetry, which lifts the degeneracy of d_{yz} and d_{zx} orbital bands: the α and β bands. As a neutron diffraction measurement has clarified,[8] the O(1)-O(1) bond of octahedra splits into a shorter one along [110] and a longer one along [110] below T_O, while the Ru-O(1) and Ru-O(2) bonds keep their lengths almost the same as those for $x=0.5$ as well as for Sr_2RuO_4. In addition, the tilt of RuO_6 octahedra occurs across the transition, which reduces the angle of the Ru-O(1)-Ru bond along [010]. Considering both the hybridization between the orbitals and the crystal field effect, the splitting in the bond length should bring about the following band degeneracy lifting, similar to the discussion in Sec. IV A: the $(d_{zx}+d_{yz})/\sqrt{2}$ orbital will form a narrower band with a lower energy, whereas the $(d_{zx}-d_{yz})/\sqrt{2}$ will generate a wider band with a higher energy, as depicted in Fig. 10. Since the lowest-energy band absorbs more electrons, the filling of the bands at E_F decreases toward one-half. Taking account of the spin-orbit coupling, this model naturally explains the in-plane anisotropy of the susceptibility in the M-M region.

Moreover, the symmetry breaking distortion may lift the degeneracy of the states piled up at the vHS of the γ band, as what is discussed for the case in the Ca substitution of $Ca_{1-x}Sr_xRuO_3$.[1,27] Therefore, due to the band splitting and the suppression of the vHS, the band at E_F will become more symmetric with smaller $N(E_F)$. This change from an asymmetric, strongly peaked band to a symmetric, half-filled band should weaken the FM coupling, but instead enhance the AF superexchange coupling in the M-M region.

In this model, the band degeneracy controls the electron filling of each band. This differs from the carrier doping to the single $d_{x^2-y^2}$ band of the high-T_c cuprates by chemical substitutions in block layers. In contrast with this type of ''real space doping,'' the filling control here may be called ''*k*-space doping.''

We note here the significant dependence on this filling of magnetic coupling, from the FM one at x_c with 2/3 filling to the AF one at $x \simeq 0.2$ with effectively half filling, while the shape of the DOS should also be vital for the switching of magnetic coupling as we discussed above. In fact, this dependence is consistent with theoretical studies by Alexander and Anderson[28] and by Moriya.[29] Based on a mean-field theory using the Anderson impurity model, they showed that the magnetic coupling switches from FM exchange to AF superexchange as the filling approaches one-half. Especially, Moriya predicted that such a switching occurs around 60% filling in the case with a simple band structure.[29] Notably, this suggests that the 2/3 filling in region III is already quite close to the critical point, as long as $N(E_F)$ is large enough, thereby with the asymmetric DOS.

Then, why does the band splitting occur below x_c instead of a FM ordering? In order to understand this, we have to take account of the orbital degree of freedom. As $N(E_F)$ increases with band narrowing, the triply degenerate bands are prone to meet a Jahn-Teller-type instability as well as a FM instability. In fact, the gap by the Jahn-Teller effect will stabilize the fourth electron in comparison with the degenerate case, and this stabilization energy becomes larger for a narrower band with higher $N(E_F)$. Therefore, we suggest that in region III, these instabilities compete with each other, and consequently the structural transition for the ground state takes over at x_c.

Moreover, orbital fluctuations and/or the dynamical Jahn-Teller effect as critical phenomena are expected on the verge of the instability point. This orbital fluctuation may lead to a nonuniform exchange interaction of spins through dynamical lifting of the orbital degeneracy. This dynamical coupling between spins and orbitals, which was recently suggested in the case of V_2O_3,[30,31] would suppress a magnetic (especially FM) long-range order at around x_c.

Across $x \approx 0.2$ into region I, the first-order structural transition occurs[2] and induces another type of orbital ordering by the Jahn-Teller effect, as we discussed in Sec. IV A. Sup-

ported by this orbital ordering, the system finally achieves AF long-range order as well as the insulating ground state.

We conclude that the interplay between the band shape control and the *k*-space doping plays a crucial role in the dramatic variation of the ground states. The development of FM coupling toward the structural transition suggests a competition between the instabilities of ferromagnetism and Jahn-Teller orbital ordering. This competition results in the band degeneracy lifting to induce the switching of magnetic coupling. The rich and unusual phenomena of the quasi-two-dimensional Mott transition system $Ca_{2-x}Sr_xRuO_4$ should help deepen our insight into the role of the orbital degree of freedom in the Mott transition mechanism as well as in itinerant magnetism.

ACKNOWLEDGMENTS

The authors acknowledge T. Ishiguro for his support in many aspects, and M. Braden and O. Friedt for an important collaboration, especially for allowing us to use some of the unpublished information. They thank H. Fukazawa, M. Minakata, and S. Ikeda for their technical support and valuable discussions. They are grateful to K. Yamada, M. Sigrist, and M. Shiga for useful discussions. This work has been supported in part by a Grant-in-Aid for Scientific Research from the Ministry of Education, Science, Sports and Culture of Japan. One of the authors (S.N.) has been supported by JSPS Research Fellowships.

[1] E.g., Y. Maeno, S. Nakatsuji, and S. Ikeda, in *Physics and Chemistry of Transition Metal Oxides*, edited by H. Fukuyama and N. Nagaosa (Springer-Verlag, Berlin, 1999), pp. 313–322.
[2] S. Nakatsuji and Y. Maeno, Phys. Rev. Lett. **84**, 2666 (2000).
[3] S. Nakatsuji *et al.* (unpublished).
[4] S. Nakatsuji, S. Ikeda, and Y. Maeno, J. Phys. Soc. Jpn. **66**, 1868 (1997).
[5] M. Braden, G. André, S. Nakatsuji, and Y. Maeno, Phys. Rev. B **58**, 847 (1998).
[6] H. Fukazawa, S. Nakatsuji, and Y. Maeno, Physica B **281&282**, 613 (2000).
[7] E.g., K. Yosida, *Theory of Magnetism* (Springer-Verlag, Berlin, 1996).
[8] O. Friedt, M. Braden, G. André, P. Adelmann, S. Nakatsuji, and Y. Maeno, cond-mat/0007218 (unpublished).
[9] C.S. Alexander, G. Cao, V. Dobrosavljevic, S. McCall, J.E. Crow, E. Lochner, and R.P. Guertin, Phys. Rev. B **60**, R8422 (1999).
[10] T. Oguchi, Phys. Rev. B **51**, 1385 (1995); D.J. Singh, *ibid.* **52**, 1358 (1995).
[11] T. Moriya, *Spin Fluctuations in Itinerant Electron Magnetism* (Springer-Verlag, Berlin, 1985).
[12] A.W. Tyler, A.P. Mackenzie, S. NishiZaki, and Y. Maeno, Phys. Rev. B **58**, R10 107 (1998).
[13] K. Yoshida, F. Nakamura, T. Goko, T. Fujita, Y. Maeno, Y. Mori, and S. NishiZaki, Phys. Rev. B **58**, 15 062 (1998).
[14] G. Soda, D. Jerome, M. Weger, J. Alizon, J. Gallice, H. Robert, J.M. Fabre, and L. Giral, J. Phys. (Paris) **38**, 931 (1977).
[15] L. Forro, V. Ilakovac, J.R. Cooper, C. Ayache, and J.-Y. Henry, Phys. Rev. B **46**, 6626 (1992).
[16] N. Kumar and A.M. Jayannavar, Phys. Rev. B **45**, 5001 (1992).
[17] The curve for $x=2$ in Fig. 9(b) is not on the universal one. This is probably caused by the fact that only Sr_2RuO_4 has no rotational distortion as we will discuss below, which results in the difference in parameters such as α and n in Eq. (3.5).
[18] As discussed below, it is owing to the flattening of the octahedra that the d_{xy} orbital will have lower energy than the other two. Therefore, the flattening is naturally explained by the Jahn-Teller effect to produce this orbital splitting, which stabilizes the fourth electron in comparison with the degenerate case.
[19] H. Mukuda, K. Ishida, Y. Kitaoka, K. Asayama, Z.Q. Mao, Y. Mori, and Y. Maeno, J. Phys. Soc. Jpn. **67**, 3945 (1998).
[20] T. Imai, A.W. Hunt, K.R. Thurber, and F.C. Chou, Phys. Rev. Lett. **81**, 3006 (1998).
[21] J. Wahle, N. Blümer, J. Schlipf, K. Held, and D. Vollhardt, Phys. Rev. B **58**, 12 749 (1998) and references therein.
[22] In addition to this basic mechanism, the local FM interaction may be stabilized by the Hund's rule coupling between moments induced on in-plane oxygen O(1) sites due to the strong covalency in Ru-O bonds, as discussed in Ref. 25.
[23] Y. Sidis, M. Braden, P. Bourges, B. Hennion, S. NishiZaki, Y. Maeno, and Y. Mori, Phys. Rev. Lett. **83**, 3320 (1999).
[24] I.I. Mazin and D.J. Singh, Phys. Rev. Lett. **82**, 4324 (1999).
[25] I.I. Mazin and D.J. Singh, Phys. Rev. Lett. **79**, 733 (1997).
[26] T. Nomura and K. Yamada, J. Phys. Soc. Jpn. **69**, 1856 (2000).
[27] I.I. Mazin and D.J. Singh, Phys. Rev. B **56**, 2556 (1997).
[28] S. Alexander and P.W. Anderson, Phys. Rev. **133**, A1594 (1964).
[29] T. Moriya, Prog. Theor. Phys. **33**, 157 (1965).
[30] M. Takigawa, E.T. Ahrens, and Y. Ueda, Phys. Rev. Lett. **76**, 283 (1996).
[31] W. Bao, C. Broholm, G. Aeppli, P. Dai, J.M. Honig, and P. Metcalf, Phys. Rev. Lett. **78**, 507 (1997).